# Resonance analysis of $^{147}$Sm($n$, $\alpha$) cross sections: Comparison to optical model calculations and indications of nonstatistical effects

P. E. Koehler*
*Physics Division, Oak Ridge National Laboratory, Oak Ridge, Tennessee 37831, USA*

Yu. M. Gledenov
*Joint Institute for Nuclear Research, Dubna, Russia*

T. Rauscher and C. Fröhlich
*Departement für Physik und Astronomie, Universität Basel, CH-4056 Basel, Switzerland*
(Received 25 July 2003; published 30 January 2004)

We have measured the $^{147}$Sm($n$, $\alpha$) cross section from 3 eV to 500 keV and performed an $\mathcal{R}$-matrix analysis in the resolved region ($E_n < 700$ eV) to extract $\alpha$ widths for 104 resonances. We computed strength functions from these resonance parameters and compared them to transmission coefficients calculated using optical model potentials similar to those employed as inputs to statistical model calculations. The statistical model often is used to predict cross sections and astrophysical reaction rates. Comparing resonance parameters rather than cross sections allows more direct tests of potentials used in the model and hence should offer greater insight into possible improvements. In particular, an improved $\alpha$+nucleus potential is needed for applications in nuclear astrophysics. In addition to providing a more direct test of the $\alpha$+nucleus potential, the $\alpha$-width distributions show indications of nonstatistical effects.

DOI: 10.1103/PhysRevC.69.015803 PACS number(s): 26.30+k, 24.60.Ky, 27.60.+j

## I. INTRODUCTION

Reactions involving $\alpha$ particles and intermediate-to-heavy mass nuclides often can play an important role in nucleosynthesis occurring in massive stars at high temperatures and in explosive environments such as supernovae [1,2]. For example, accurate rates for many ($\gamma$, $\alpha$) reactions are needed for a better understanding of the nucleosynthesis of the neutron deficient $A > 90$ nuclides during the so-called $p$ process. As important as these reactions are, there is scant experimental information on their rates because the cross sections are extremely small and many of the required "target" isotopes have very small natural abundances (and hence are very expensive) or are radioactive; thus, direct measurements are very difficult. However, most of the required rates should be calculable to sufficient accuracy using the nuclear statistical model, but these theoretical calculations are, at present, hampered by large uncertainties in the $\alpha$+nucleus potential in the astrophysically relevant energy range.

We recently [3] have shown that ($n$, $\alpha$) cross section measurements on intermediate-to-heavy mass nuclides offer perhaps the best means for constraining the many parameters defining a realistic $\alpha$+nucleus potential. Although this approach is showing great promise, one drawback is that the comparison between theory and experiment as cross sections involves sensitivity to other model parameters in addition to the $\alpha$+nucleus potential. A more direct comparison of $\alpha$ strength functions extracted from the measurements to theoretical expectations should avoid these confounding dependencies and allow greater insight into possible improvements in the model.

$^{147}$Sm appears to be the best candidate for such a study for several reasons. First, the $Q$ value for $^{147}$Sm($n$, $\alpha$) is fairly large, so the cross section, although still very small, is expected to be among the largest in this mass range. Second, the natural abundance of $^{147}$Sm is fairly large, so the necessary isotopically enriched sample is affordable. Third, unlike several other potential candidates, there is relatively complete information on the parameters for the 100 lowest-energy resonances. This is important because reliably extracting $\alpha$ widths requires reasonably complete knowledge of the neutron and $\gamma$ widths for the resonances, and comparison to theory is most meaningful if the spins and parities of the resonances are known. For $s$-wave neutrons incident on $^{147}\mathrm{Sm}\left(I^{\pi}=\frac{7}{2}^{-}\right)$, $J^{\pi}=3^{-}$ and $4^{-}$ resonances can be formed in the compound nucleus $^{148}$Sm.

The $\alpha$ widths for several $^{147}$Sm($n$, $\alpha$) resonances for $E_n < 700$ eV were determined in previous measurements [4–8] of this cross section, and these data were compared to statistical model predictions. However, these comparisons were hampered by the fact that the $\alpha$ widths for most of the resonances in this region could not be measured. We have employed an improved detector to make a new measurement of the $^{147}$Sm($n$, $\alpha$) cross section. In addition to extending the range of the measurements to much higher energies, this new detector resulted in a much improved signal-to-noise ratio in the resolved resonance region so that the $\alpha$ widths for most of the resonances in this region could be extracted from the data. This much improved $\alpha$-width information makes possible a more meaningful comparison between theory and experiment.

## II. EXPERIMENT

The experiment has been described elsewhere [3,9], so only the salient features will be given here. The measure-

*Electronic address: koehlerpe@ornl.gov

 

ments were made at the Oak Ridge Electron Linear Accelerator (ORELA) [10–12] white neutron source. The ORELA was operated at a repetition rate of 525 Hz, a power of 6–8 kW and a pulse width of 8 ns. A 0.76-mm thick Cd filter was used to eliminate the overlap of slow neutrons from previous pulses and a 1.27-cm thick Pb filter was used to help reduce overload effects from the $\gamma$ flash at the start of each neutron pulse. Neutron energies were measured via time of flight. The detector was a compensated ionization chamber (CIC) [13]. Although a CIC can have poorer pulse-height resolution than, for example, a gridded ionization chamber, it reduces overload effects due to the $\gamma$ flash at the start of each neutron pulse by several orders of magnitude, allowing measurements to be made with excellent signal-to-noise ratio to much higher neutron energies (500 keV in the present case).

The source-to-sample distance was 8.835 m and the neutron beam was collimated to 10 cm in diameter at the sample position. Two samples were placed back-to-back in the center of our parallel-plate CIC with the planes of the samples perpendicular to the neutron beam. Hence, the cross section was measured over nearly the entire $4\pi$ solid angle. The samples were in the form of $Sm_2O_3$ enriched to 95.3% in $^{147}$Sm and were 5.0 mg/cm$^2$ thick by 11 cm in diameter. The $^6$Li$(n, \alpha)^3$H reaction was used to measure the energy dependence of the flux and to normalize the raw counts to absolute cross section. These measurements were made during a run when one of the $^{147}$Sm samples was replaced by a $^6$Li sample. The neutron energy scale also was calibrated during this run using dips in the time-of-flight spectrum caused by resonances in the Cd filter and Al vacuum windows in the flight path as well as the peak due to the 244.5-keV resonance from the $^6$Li$(n, \alpha)^3$H reaction. A $^6$Li sample in a separate parallel-plate CIC was used as a flux monitor. The most recent ENDF evaluation [14] for the $^6$Li$(n, \alpha)^3$H reaction was used in calculating the absolute cross sections. The data were corrected for the small background due to the spontaneous $\alpha$ decay of $^{147}$Sm and for the effects of $\alpha$ straggling in the samples. This latter correction (14%) was calculated using the computer code SRIM [15]. The overall normalization uncertainty of $\approx$6% is dominated by the uncertainty ($\pm$4%) in this correction and by uncertainties ($\pm$3%) in the sample sizes.

## III. RESONANCE ANALYSIS AND RESULTS

The data were fitted with the $\mathcal{R}$-matrix code SAMMY [16] to extract the $\alpha$ widths for resonances in the resolved region below 700 eV. Almost all observed [17] resonances in this energy range have been assigned [18] as $J^\pi = 3^-$ or $4^-$ ($s$ wave). A radius of 8.3 fm was used in all $^{147}$Sm channels. Both the fact that the sample was an oxide and the aluminum backing were included in the input files for SAMMY so that corrections could be applied for attenuation and multiple-scattering effects in the sample and its backing. The resonance energies, spins, parities, and neutron and $\gamma$ widths from the compilation of Ref. [17], which are based mainly on the work of Refs. [18–21], were used as starting values in the analysis. Only a few of the energies had to be adjusted, and one (tentative) spin assignment (for the 659.4-eV resonance) was changed to fit the data. A radiation width equal to the average for $^{147}$Sm resonances (69 meV Refs. [17,22]) was used for resonances without $\Gamma_\gamma$ values in Ref. [17]. The resulting parameters are given in Table I where, for example, 1.273 *(61)* is used to denote $1.273 \pm 0.061$, etc. Representative plots of the data and $\mathcal{R}$-matrix fits are shown in Fig. 1.

The accuracy of the extracted $\alpha$ widths depends on the accuracy of the $J^\pi$, $\Gamma_n$, and $\Gamma_\gamma$ assignments for the resonances because our measurement technique determines only the resonance areas, $A_\alpha = g_J \Gamma_\alpha \Gamma_n / \Gamma$, where $g_J$ is the statistical factor **(**$g_J = (2J+1)/[(2I+1)(2i+1)]$, where $J$, $I$, and $i$ are the spins of the resonance, $^{147}$Sm, and the neutron, respectively**)**. The uncertainties in the resonance areas in Table I are the one-standard-deviation uncertainties determined in fitting the data. The uncertainties in the $\alpha$ widths include additional contributions (added in quadrature) from the uncertainties in the neutron and radiation widths. The uncertainties in the neutron and radiation widths were taken from Ref. [17]. For resonances with unknown radiation widths a "factor of 2" ($\pm$23 meV) uncertainty was assumed, which should be a conservative overestimate of the uncertainty because the measured radiation widths [18,21] show very little variability.

For 23 of the 104 resonances in this region, the fitted resonance areas had a relative uncertainty greater than 70%. In these cases we give only upper limits for the resonance areas in Table I equal to the fitted values plus the one-standard-deviation uncertainties determined by SAMMY. The upper limits on the $\alpha$ widths given in Table I for these cases were calculated from the upper limits on the resonance areas using the listed spins and neutron and radiation widths. The uncertainties in the neutron and radiation widths have negligible effects in these cases and hence were not taken into account when calculating these $\alpha$-width upper limits.

### A. Average resonance parameters

For comparison to statistical model calculations, distributions or averages of resonance parameters are needed. Some of these quantities were determined from a resonance analysis of the total cross section [21]. With the resonance spin and $\gamma$-width information from Ref. [18] and the $\alpha$-width information from this work, it is possible to calculate these quantities for each of the two possible spin states for $s$-wave resonances and to include the $\alpha$ channels as well as the neutron channels. Useful quantities for comparison to statistical model calculations include strength functions $S$, average level spacings $D$, average widths $\langle\Gamma\rangle$, and the distributions of widths (see Sec. VI for a detailed discussion of these quantities). Care must be taken into account for effects due to missed resonances.

#### *1. Neutron and $\gamma$ channels*

The $s$-wave neutron strength function, $S_0 = \langle\Gamma_n^0\rangle / D_0$, where $\langle\Gamma_n^0\rangle$ is the average $s$-wave reduced neutron width ($\Gamma_n = \Gamma_n^0 \times \sqrt{E_n}$) and $D_0$ is the average $s$-wave level spacing, can be determined from the slope of a plot of the cumulative reduced neutron width versus resonance energy resulting from

TABLE I. $^{147}$Sm($n$, $\alpha$) resonance parameters.

| $E_n$ (eV) | $J^\pi$ | $2g\Gamma_n$ (meV) | $\Gamma_\gamma$ (meV) | $\Gamma_\alpha$ ($\mu$eV) | $g\Gamma_n\Gamma_\alpha/\Gamma$ ($\mu$eV) |
|---|---|---|---|---|---|
| 3.397 | $3^-$ | 1.18 *(2)* | 67 *(3)* | 1.273 *(61)* | 0.010898 *(94)* |
| 18.340 | $4^-$ | 80.9 *(4)* | 72 *(4)* | 0.2789 *(90)* | 0.0784 *(12)* |
| 27.218 | $3^-$ | 6.08 *(11)* | 84 *(5)* | 0.420 *(37)* | 0.01403 *(93)* |
| 29.791 | $3^-$ | 12.9 *(2)* | 71 *(6)* | 0.543 *(44)* | 0.0408 *(15)* |
| 32.151 | $4^-$ | 43.9 *(6)* | 70 *(5)* | 0.276 *(16)* | 0.0556 *(18)* |
| 39.700 | $4^-$ | 80.2 *(11)* | 68 *(4)* | 0.289 *(13)* | 0.0833 *(27)* |
| 40.720 | $3^-$ | 4.7 *(2)* | 69 | 0.44 *(14)* | 0.0140 *(13)* |
| 49.358 | $4^-$ | 16.5 *(3)* | 75 *(4)* | 0.256 *(24)* | 0.0236 *(19)* |
| 58.130 | $3^-$ | 35.9 *(6)* | 77 *(5)* | 0.556 *(36)* | 0.0845 *(39)* |
| 64.96 | $(4)^-$ | 7.4 *(4)* | 69 | 0.40 *(14)* | 0.0195 *(38)* |
| 65.13 | $(3)^-$ | 4.8 *(3)* | 69 | 0.14 *(10)* | 0.0046 *(29)* |
| 76.15 | $4^-$ | 19.7 *(6)* | 74 *(5)* | 0.208 *(34)* | 0.0224 *(34)* |
| 79.89 | $4^-$ | 4.2 *(3)* | 69 | 0.27 *(14)* | 0.0079 *(30)* |
| 83.775 | $3^-$ | 65.8 *(15)* | 76 *(5)* | 3.55 *(16)* | 0.772 *(16)* |
| 94.90 | $(4^-)$ | 5.6 *(4)* | 69 | $<$0.018 | $<$0.00065 |
| 99.54 | $4^-$ | 263 *(4)* | 79 *(5)* | 0.034 *(12)* | 0.0142 *(51)* |
| 102.80 | $3^-$ | 173.6 *(31)* | 76 *(7)* | 1.486 *(70)* | 0.470 *(15)* |
| 107.06 | $4^-$ | 49.7 *(16)* | 82 *(5)* | 1.100 *(81)* | 0.217 *(11)* |
| 108.58 | $4^-$ | 1.0 *(4)* | 69 | $<$1.2 | $<$0.0077 |
| 123.95 | $3^-$ | 151.5 *(33)* | 73 *(6)* | 1.276 *(71)* | 0.392 *(17)* |
| 140.30 | $3^-$ | 77.7 *(21)* | 69 | 0.78 *(13)* | 0.192 *(14)* |
| 143.27 | $4^-$ | 3.6 *(5)* | 69 | $<$0.72 | $<$0.017 |
| 151.54 | $3^-$ | 144 *(4)* | 75 *(5)* | 0.528 *(52)* | 0.159 *(14)* |
| 161.03 | $3^-$ | 47.6 *(21)* | 69 | 4.04 *(82)* | 0.780 *(48)* |
| 161.88 | $4^-$ | 15.6 *(12)* | 69 | 5.6 *(17)* | 0.523 *(48)* |
| 163.62 | $4^-$ | 175 *(4)* | 77 *(4)* | 0.342 *(59)* | 0.129 *(22)* |
| 171.80 | $4^-$ | 18.5 *(11)* | 69 *(4)* | 0.35 *(11)* | 0.038 *(11)* |
| 179.68 | $3^-$ | 9.0 *(9)* | 69 | 1.92 *(67)* | 0.109 *(18)* |
| 184.76 | $3^-$ | 356 *(6)* | 69 | 20.9 *(11)* | 7.83 *(10)* |
| 191.07 | $3^-$ | 31.5 *(16)* | 79 *(5)* | 3.09 *(30)* | 0.423 *(30)* |
| 193.61 | $4^-$ | 5.6 *(10)* | 69 | $<$0.53 | $<$0.019 |
| 198.03 | $3^-$ | 13.7 *(12)* | 61 *(4)* | $<$0.034 | $<$0.0030 |
| 206.03 | $4^-$ | 207 *(5)* | 83 *(5)* | $<$0.043 | $<$0.017 |
| 221.03 | $3^-$ | 118 *(4)* | 67 *(6)* | 0.98 *(16)* | 0.286 *(46)* |
| 222.68 | $3^-$ | 224 *(6)* | 86 *(5)* | 2.47 *(20)* | 0.808 *(58)* |
| 225.91 | $(3^-)$ | 2.9 *(13)* | 69 | 11.1 *(63)* | 0.222 *(31)* |
| 228.48 | $4^-$ | 1.7 *(4)* | 69 | $<$1.8 | $<$0.021 |
| 240.76 | $4^-$ | 19.1 *(18)* | 91 *(6)* | 0.37 *(18)* | 0.033 *(16)* |
| 247.62 | $4^-$ | 163 *(6)* | 69 *(6)* | 0.137 *(52)* | 0.052 *(19)* |
| 257.13 | $3^-$ | 82 *(4)* | 69 | 0.60 *(11)* | 0.152 *(26)* |
| 263.57 | $3^-$ | 65 *(4)* | 69 | 0.41 *(13)* | 0.092 *(26)* |
| 266.26 | $4^-$ | 204 *(7)* | 72 *(6)* | $<$0.17 | $<$0.069 |
| 270.72 | $3^-$ | 76 *(4)* | 85 *(6)* | 0.97 *(16)* | 0.213 *(34)* |
| 274.40 | $3^-$ | 19.1 *(23)* | 69 | 2.65 *(82)* | 0.279 *(36)* |
| 283.28 | $4^-$ | 22.8 *(25)* | 58 *(10)* | $<$0.14 | $<$0.021 |
| 290.10 | $(4)^-$ | 41.3 *(33)* | 68 *(6)* | 0.53 *(15)* | 0.105 *(27)* |
| 308.30 | $3^-$ | 8.3 *(20)* | 69 | $<$0.51 | $<$0.026 |
| 312.06 | $4^-$ | 27.6 *(26)* | 69 | 0.41 *(22)* | 0.060 *(29)* |
| 321.13 | $3^-$ | 11.4 *(11)* | 69 | $<$0.46 | $<$0.031 |
| 330.10 | $3^-$ | 67 *(4)* | 69 | 0.41 *(22)* | 0.095 *(47)* |
| 332.10 | $4^-$ | 73 *(4)* | 69 | $<$0.39 | $<$0.10 |
| 340.4 | $4^-$ | 178 *(7)* | 69 | 0.18 *(11)* | 0.070 *(41)* |
| 349.86 | $3^-$ | 68 *(4)* | 69 | 0.38 *(19)* | 0.088 *(43)* |
| 359.32 | $4^-$ | 402 *(12)* | 69 | 0.28 *(11)* | 0.131 *(52)* |
| 362.15 | $4^-$ | 31 *(4)* | 69 | $<$0.49 | $<$0.077 |
| 379.2 | $4^-$ | 393 *(12)* | 69 | 0.72 *(20)* | 0.340 *(90)* |
| 382.4 | $3^-$ | 139 *(8)* | 69 | 1.28 *(44)* | 0.39 *(13)* |
| 385.16 | $4^-$ | 122 *(7)* | 69 | 3.70 *(67)* | 1.27 *(13)* |
| 396.5 | $(4)^-$ | 67 *(5)* | 69 | 0.54 *(33)* | 0.141 *(81)* |
| 398.6 | $3^-$ | 109 *(7)* | 69 | 0.41 *(24)* | 0.116 *(67)* |
| 405.1 | $3^-$ | 34 *(4)* | 69 | 1.13 *(48)* | 0.178 *(61)* |
| 412.0 | $3^-$ | 55 *(5)* | 69 | $<$0.49 | $<$0.10 |
| 418.3 | $(4)^-$ | 235 *(12)* | 69 | 0.43 *(18)* | 0.180 *(74)* |
| 421.8 | $4^-$ | 68 *(5)* | 69 | 0.73 *(32)* | 0.193 *(75)* |
| 433.1 | $(3^-)$ | 17 *(4)* | 69 | 2.8 *(17)* | 0.26 *(13)* |
| 435.7 | $3^-$ | 154 *(9)* | 69 | 1.94 *(63)* | 0.61 *(18)* |
| 439.5 | $4^-$ | 40 *(5)* | 69 | 9.5 *(26)* | 1.81 *(17)* |
| 446.9 | $3^-$ | 7 *(3)* | 69 | $<$1.59 | $<$0.067 |
| 458.6 | $4^-$ | 100 *(7)* | 69 | 0.24 *(16)* | 0.077 *(50)* |
| 462.9 | $3^-$ | 53 *(6)* | 69 | $<$0.30 | $<$0.061 |
| 476.0 | $4^-$ | 117 *(8)* | 69 | 0.41 *(25)* | 0.140 *(82)* |
| 479.8 | $3^-$ | 177 *(11)* | 69 | 1.43 *(39)* | 0.47 *(11)* |
| 486.4 | $3^-$ | 111 *(8)* | 69 | 1.70 *(43)* | 0.48 *(10)* |
| 496.2 | $4^-$ | 120 *(9)* | 69 | 0.28 *(20)* | 0.096 *(68)* |
| 498.6 | $(3)^-$ | 294 *(15)* | 69 | 0.41 *(23)* | 0.150 *(83)* |
| 518.2 | $4^-$ | 474 *(20)* | 69 | 1.92 *(30)* | 0.93 *(13)* |
| 528.9 | $4^-$ | 72 *(7)* | 69 | 0.34 *(23)* | 0.093 *(60)* |
| 532.5 | $3^-$ | 60 *(7)* | 69 | 0.42 *(30)* | 0.091 *(62)* |
| 538.1 | $4^-$ | 575 *(22)* | 69 | 0.64 *(23)* | 0.32 *(11)* |
| 546.0 | $(3)^-$ | 185 *(12)* | 69 | 0.85 *(34)* | 0.28 *(11)* |
| 553.2 | $3^-$ | 367 *(26)* | 69 | 0.33 *(22)* | 0.125 *(83)* |
| 554.5 | $4^-$ | 248 *(20)* | 69 | 1.77 *(45)* | 0.76 *(17)* |
| 559.7 | $3^-$ | 207 *(14)* | 69 | 0.82 *(44)* | 0.28 *(15)* |
| 563.4 | $4^-$ | 219 *(15)* | 69 | 1.39 *(55)* | 0.58 *(22)* |
| 567.6 | $(3^-)$ | 38 *(7)* | 69 | 4.5 *(17)* | 0.76 *(19)* |
| 574.3 | $4^-$ | 101 *(9)* | 69 | 2.37 *(64)* | 0.75 *(15)* |
| 580.2 | $3^-$ | 124 *(11)* | 69 | 0.29 *(20)* | 0.085 *(57)* |
| 587.8 | $3^-$ | 83 *(9)* | 69 | 0.95 *(46)* | 0.24 *(11)* |
| 597.4 | $4^-$ | 176 *(13)* | 69 | 0.52 *(27)* | 0.20 *(10)* |
| 606.0 | $4^-$ | 126 *(11)* | 69 | 0.56 *(32)* | 0.19 *(11)* |
| 612.6 | $(3^-)$ | 93 *(10)* | 69 | 1.13 *(59)* | 0.30 *(15)* |
| 617.2 | $(3)^-$ | 493 *(25)* | 69 | $<$0.97 | $<$0.38 |
| 622.6 | $(3^-)$ | 151 *(13)* | 69 | 0.66 *(41)* | 0.21 *(13)* |
| 625.3 | $(4^-)$ | 74 *(10)* | 69 | $<$1.1 | $<$0.28 |

TABLE I. (*Continued.*)

| $E_n$ (eV) | $J^\pi$ | $2g\Gamma_n$ (meV) | $\Gamma_\gamma$ (meV) | $\Gamma_\alpha$ ($\mu$eV) | $g\Gamma_n\Gamma_\alpha/\Gamma$ ($\mu$eV) |
|---|---|---|---|---|---|
| 634.0 | $3^-$ | 29 *(8)* | 69 | 1.8 *(1.1)* | 0.26 *(12)* |
| 644.7 | $(3^-)$ | 60 *(9)* | 69 | 0.92 *(56)* | 0.20 *(11)* |
| 648.5 | $(3^-)$ | 209 *(15)* | 69 | <0.40 | <0.14 |
| 651.9 | $(4^-)$ | 102 *(11)* | 69 | 2.16 *(77)* | 0.69 *(21)* |
| 659.4 | $(3)^-$ | 80 *(10)* | 69 | 5.9 *(16)* | 1.48 *(26)* |
| 667.0 | $4^-$ | 65 *(10)* | 69 | 15.6 *(41)* | 4.00 *(34)* |
| 677.5 | $(3^-)$ | 159 *(14)* | 69 | <0.48 | <0.15 |
| 683.1 | $(4^-)$ | 236 *(18)* | 69 | <0.29 | <0.12 |
| 687.4 | $(3^-)$ | 19 *(9)* | 69 | <2.6 | <0.24 |
| 697.0 | $(4)^-$ | 87 *(12)* | 69 | <1.5 | <0.44 |

a resonance analysis of total cross section measurements. This well-known technique for determining the neutron strength function is relatively insensitive to missing resonances because only resonances having small neutron widths are expected to be missed in total cross section measurements and the slope of the cumulative reduced neutron width versus resonance energy is little affected by missing resonances with small widths. In Ref. [21], this technique was

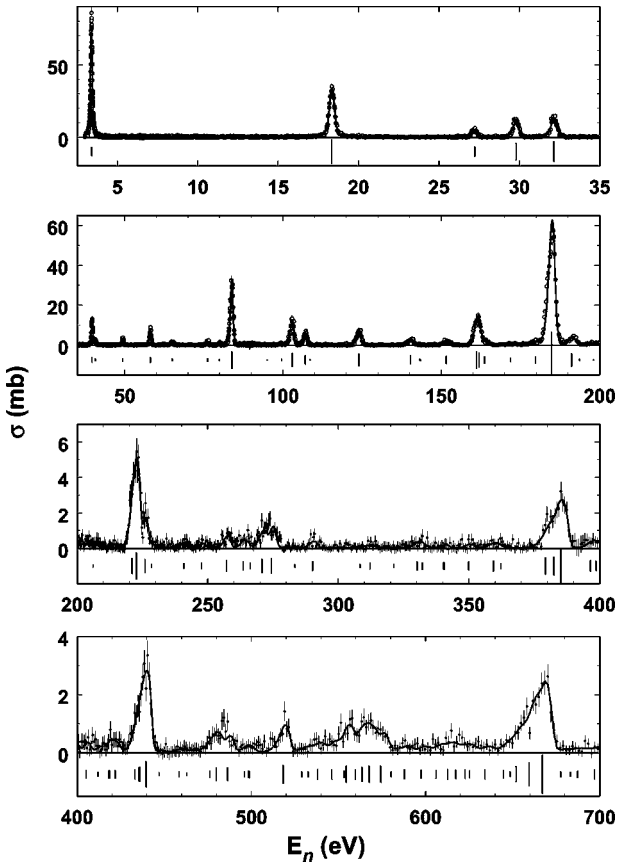


FIG. 1. $^{147}$Sm($n$, $\alpha$) cross section data (points with error bars) and SAMMY fit (solid curves). Bars below the data show the locations of the fitted resonances. The length of each bar is proportional to the square root of the resonance area.

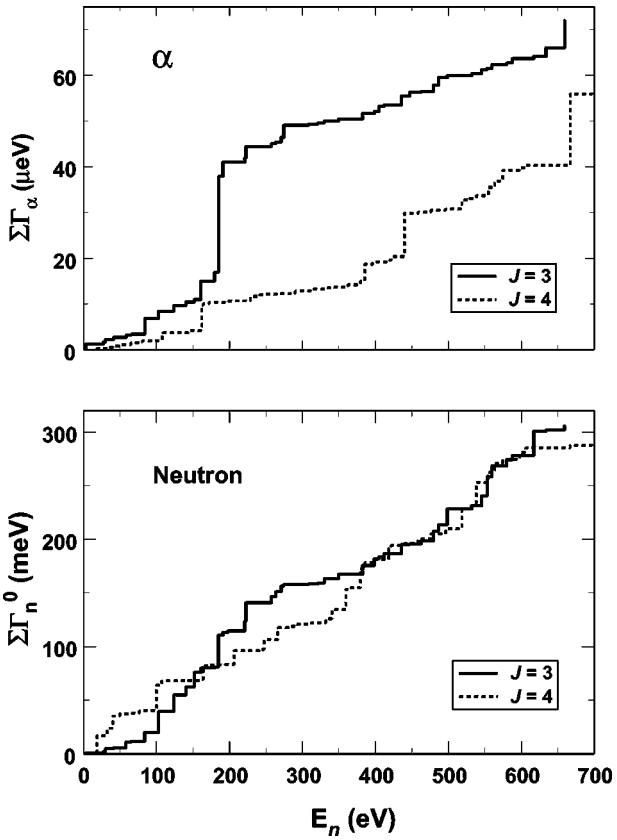


FIG. 2. Strength function plots for the $\alpha$ (top) and neutron (bottom) channels. Solid and dashed staircase plots represent results for $3^-$ and $4^-$ resonances, respectively. The measured strength functions are equal to the slopes of these staircase plots.

used to calculate $10^4 S_0 = 4.8 \pm 0.5$. Using the resonance spin information from Ref. [18] together with the neutron widths from Ref. [21], strength function plots for the two possible *s*-wave spins were constructed and are shown in Fig. 2. Linear fits to the data in Fig. 2 yield strength functions of $(4.6 \pm 1.0) \times 10^{-4}$ and $(4.3 \pm 0.9) \times 10^{-4}$ for $J=3$ and 4 resonances, respectively, in agreement with the combined *s*-wave strength function of Ref. [21]. Uncertainties in the strength functions were estimated from the number of observed resonances as described in Ref. [23].

In Ref. [21], the well-known technique of determining the level spacing from the inverse of the slope of the cumulative number of resonances versus resonance energy (in the lower energy region where missed resonances are insignificant) was used to calculate an average level spacing $D_0 = 5.7 \pm 0.5$ eV for all *s*-wave resonances. Using this level spacing and assuming that the number of resonances for each spin is proportional to $2J+1$, leads to $N=54$ and 69 resonances by 700 eV for $J=3$ and 4 resonances, respectively (implying $D_0 = 13.0$ and 10.1 eV for $J=3$ and 4 resonances, respectively). These level spacings, together with the above strength functions for $J=3$ and 4, yield $\langle \Gamma_n^0 \rangle = 5.98$ and 4.4 meV, for $J=3$ and 4 resonances, respectively.

Neutron widths are expected to obey Porter-Thomas [24] distributions having average widths and numbers of resonances consistent with the above strength function and level

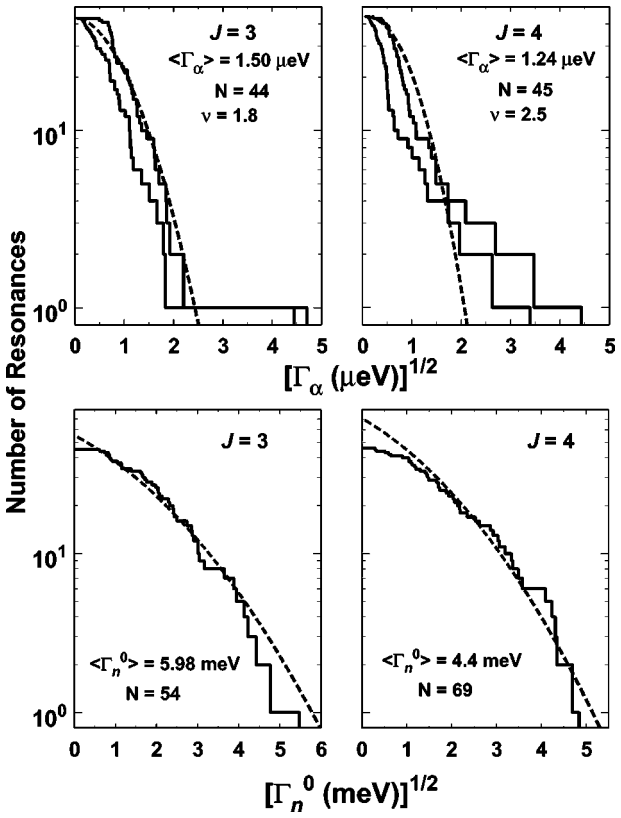


FIG. 3. Integral distributions of total $\alpha$ (top) and reduced neutron (bottom) widths for $3^-$ (left) and $4^-$ (right) resonances in $^{147}$Sm. The histograms show the measured number of resonances having widths greater than a given width vs that width. In an attempt to depict the experimental uncertainties, histograms for the $\alpha$ widths are plotted at the measured widths plus and minus their respective uncertainties. The dashed curves show the expected $\chi^2$ distributions for the average widths, number of resonances, and degrees of freedom ($\nu$=1 for neutrons) indicated.

spacing determinations. This was found to be the case in Ref. [21] for all (sum of $J$=3 and 4) $s$-wave resonances. The separate neutron width distributions for $J$=3 and 4 resonances are shown in Fig. 3. We will discuss how well they compare to the expected Porter-Thomas distributions in Sec. V.

### *2. α channel*

Our measurement technique is sensitive to resonance areas, $A_\alpha = g_J \Gamma_\alpha \Gamma_n / \Gamma$; hence, missed resonances can have small as well as large (e.g., when $\Gamma_n$ is small) $\alpha$ widths. Therefore, determining the $\alpha$ strength functions from the slopes of the cumulative $\alpha$ widths versus neutron energy (top part of Fig. 2), will likely result in values that are systematically small. On the other hand, because missed resonances should have a range of $\alpha$ widths, the average $\alpha$ widths should be less affected by associated systematic effects and strength functions calculated from the average widths should be more reliable. There is the additional complication that the data indicate that the average $\alpha$ widths as well as the $\alpha$ strength functions show considerable variations as functions of energy. For example, as shown in Fig. 2, there are large steps in the slopes

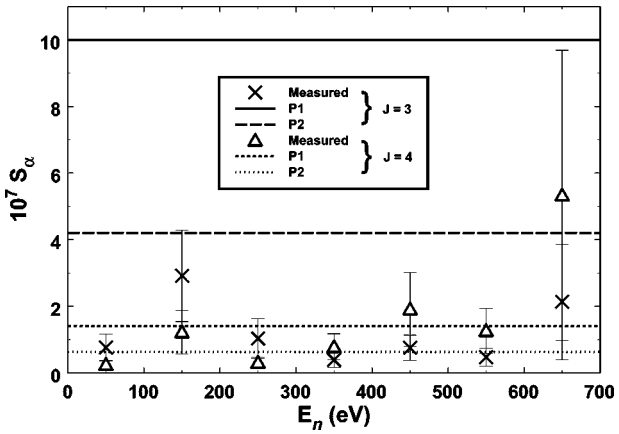


FIG. 4. Measured $\alpha$ strength functions averaged over 100-eV intervals for $J^\pi = 3^-$ ($X$'s) and $4^-$ (triangles) resonances. Strength functions for $J^\pi = 3^-$ resonances calculated with the standard ($P1$) and modified ($P2$) NON-SMOKER parameters are shown as solid and long-dashed lines, respectively, whereas corresponding calculations for $J^\pi = 4^-$ resonances are shown as short-dashed and dotted lines, respectively.

of the cumulative $\alpha$ widths versus neutron energy. For this reason, the $\alpha$ strength functions were calculated over different energy intervals. As shown in Fig. 4, the $\alpha$ strength functions calculated from the $\alpha$ widths ($S = \langle\Gamma\rangle / D$) averaged over 100-eV intervals show considerable variation. In addition, as shown in Fig. 5, the ratio of the $\alpha$ strength functions for the two different $s$-wave spins states changes dramatically near 300 eV. Because it is possible that this effect is caused by incorrect spin assignments and because the strength functions as well as their ratio are relatively constant in the 0–300 eV and 300–600 eV intervals, we list the strength functions calculated for these two ranges as well as for the entire 0–600 eV interval in Table II. We did not include the 600–700 keV interval because there are only about half as many resonances having firm $J^\pi$ assignments in this energy range as in the six lower-energy bins. We compare these values to statistical model calculations in Sec. VI.

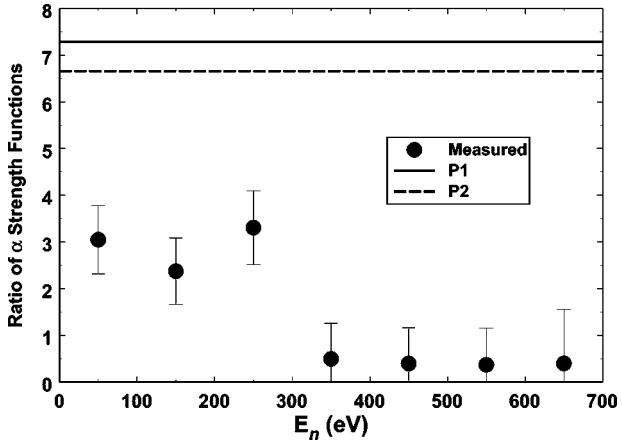


FIG. 5. Ratios ($J^\pi = 3^-$ to $4^-$ resonances) of $\alpha$ strength functions averaged over 100-eV intervals. Measured ratios are shown as solid circles. Ratios calculated with the standard ($P1$) and modified ($P2$) NON-SMOKER parameters are shown as solid and long-dashed lines, respectively.

TABLE II. Neutron and $\alpha$ strength functions from experiment and optical models.

| $J$ | Neutrons $10^4 S_0$ | | Alphas $10^6 S_\alpha$ | | | | |
|---|---|---|---|---|---|---|---|
| | Experiment | Optical model | Experiment | | | Optical model | |
| | | | 0–600 eV | 0–300 eV | 300–600 eV | $P1$ | $P2$ |
| 3 | 4.6±1.0 | 9.2 | 0.116±0.025 | 0.171±0.052 | 0.0560±0.018 | 1.0 | 0.42 |
| 4 | 4.3±0.9 | 9.2 | 0.092±0.020 | 0.058±0.018 | 0.127±0.039 | 0.14 | 0.063 |

Distributions of $\alpha$ widths for the two $s$-wave spin states are shown in Fig. 3. $\alpha$ widths for transitions to individual final states are expected to obey Porter-Thomas distributions, but we were unable to resolve individual $\alpha$ groups because our samples were too thick. Therefore, the $\alpha$-width distributions are convolutions of Porter-Thomas distributions. This will be discussed more fully in Sec. V.

## IV. COMPARISON TO PREVIOUS WORK

There is reasonably good agreement between the $\alpha$ widths we determined and previous work (as compiled in Ref. [17]) except that we have many more measured widths and hence many fewer upper limits. There are however at least two important differences between previous results and the resonance parameters reported herein. First, the neutron and $\gamma$ widths used to extract the $\alpha$ widths typically were not reported in previous work. Because the $\alpha$ widths extracted can vary substantially depending on the values of these other parameters, comparisons to previously reported $\alpha$ widths without this information are of limited value. Second, originally [25], we followed the example of Ref. [7] and assigned the stronger peaks in our data to the same resonances they used even though, as the energy increased, our energy scale indicated that the peaks actually corresponded to the next higher-energy resonances. As a result, our resonance energies became increasingly larger than those of Ref. [17] as the energy increased. For example, with this scheme the resonance we observed at 439.5 eV would correspond to the resonance in Ref. [17] at 435.7 eV rather than to the much closer resonance at 440.2 eV. After a recheck of our energy calibration, using the present data as well as data from $^{143}$Nd($n$, $\alpha$) [26] and $^{95}$Mo($n$, $\alpha$) [9] measurements run under the same conditions using the same apparatus, we decided that it was not possible for our energy scale to be wrong in this manner. Therefore, we assigned the resonances we observed to the closest ones in Ref. [17]. As a result, many of the spin assignments as well as the extracted $\alpha$ widths (because the widths were calculated using the wrong spins and neutron and radiation widths) in our preliminary report [25] are incorrect, and several resonances with large $\alpha$ widths at the higher energies are now assigned to $J^\pi=4^-$ rather than $J^\pi=3^-$.

Further evidence that our spin assignments are correct can be seen in the pulse-height distributions for the resonances. As illustrated in Fig. 6, because parity must be conserved, $4^-$ resonances in $^{148}$Sm are forbidden from decaying to the $0^+$ ground state of $^{144}$Nd by $\alpha$ emission, whereas $3^-$ resonances are not. Therefore, the pulse-height spectrum for $\alpha$ particles from $4^-$ resonances will not include the highest-energy group corresponding to decay to the ground state of $^{144}$Nd. Because our samples were relatively thick, we could not resolve the various $\alpha$-particle groups. However, as shown in Fig. 7, there is a discernible difference between the pulse-height spectra for unambiguously assigned $J^\pi=3^-$ and $4^-$ resonances. As expected, the $J^\pi=3^-$ resonance at 83.775 eV occurs at larger pulse height than the $J^\pi=4^-$ resonance at 18.340 eV. This figure also demonstrates that the pulse height spectrum corresponding to the resonance at 667.0 eV clearly favors a $4^-$ assignment for this resonance. Similar comparisons show that $4^-$ assignments also are favored for several other resonances with fairly large $\alpha$ widths which had been associated with $3^-$ resonances in previous work [7], lending confidence that the energy calibration, and therefore the spin assignments, of the present work are correct.

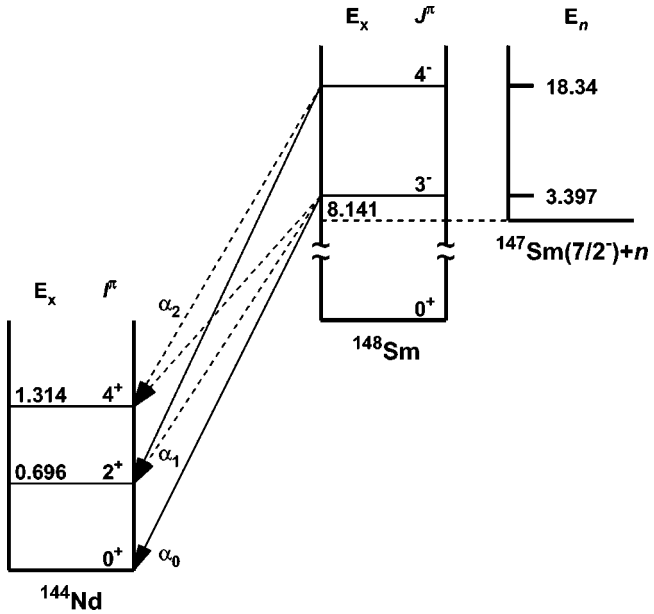


FIG. 6. Energy-level diagrams depicting the $^{147}$Sm($n$, $\alpha$)$^{144}$Nd reaction ($Q$=10.127 MeV). Excitation energies $E_x$ are given in mega electron volt, whereas laboratory neutron energies $E_n$ are given in electron volt. The energy scales of the $^{144}$Nd and $^{148}$Sm parts of the figure differ by a factor of 17 million. $J^\pi=3^-$ levels in $^{148}$Sm can $\alpha$ decay to the ground as well as excited (with substantially reduced penetrability) states of $^{144}$Nd. $J^\pi=4^-$ levels in $^{148}$Sm are parity forbidden from decaying to the ground state of $^{144}$Nd, but can decay to excited states.

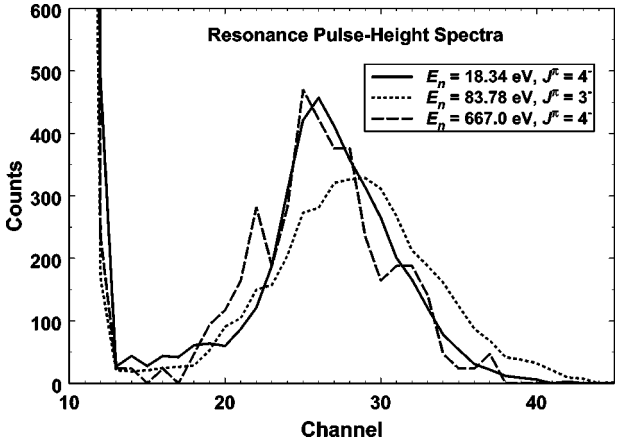


FIG. 7. Pulse-height spectra from the $^{147}$Sm($n$, $\alpha$) reaction for the 18.340-, 83.775-, and 667.0-eV resonances. The spectra have been normalized to have equal areas.

## V. POSSIBLE NONSTATISTICAL EFFECTS

Analysis of previous $^{147}$Sm($n$, $\alpha$) measurements [4,5,7] have hinted at the possible presence of nonstatistical effects. The improved precision and accuracy of the current measurements together with improved resonance parameter information [18] makes it possible to perform more robust tests for nonstatistical effects.

In nuclear statistical theory, partial widths $\Gamma$ associated with the decay of compound nuclear states are assumed to be described by $\chi^2$ distributions with $\nu$ degrees of freedom,

$$P(x,\nu) = \frac{\nu}{2G(\nu/2)}\left(\frac{\nu x}{2}\right)^{\nu/2-1}\exp\left(-\frac{\nu x}{2}\right), \qquad (1)$$

where $G$ is the $\gamma$ function, $x=\Gamma/\langle\Gamma\rangle$, $\langle\Gamma\rangle$ is the average width, and the distribution is characterized by a dispersion equal to $2\langle\Gamma\rangle^2/\nu$. Neutron widths as well as partial $\alpha$ widths for specific angular momentum values to individual final states are expected to have $\nu=1$, and hence obey Porter-Thomas [24] distributions. On the other hand, $\gamma$ widths show much smaller fluctuations because the much larger number of decay channels in the $\gamma$-ray cascade implies a $\chi^2$ distribution with many more degrees of freedom. In our present experiment, we were unable to resolve the individual $\alpha$ groups, and hence only the total $\alpha$ widths summed over the various possible final states were measured. Because the partial $\alpha$ widths fluctuate independently, the fluctuations of the total $\alpha$ widths, $\Gamma_\alpha=\Sigma\Gamma_{\alpha c}$, are expected to be smaller owing to random cancellations of the partial widths. Therefore, the distributions of total $\alpha$ widths are expected to be narrower ($\nu>1$) than for the partial widths. The distribution for total $\alpha$ widths are complicated convolutions of partial distributions with $\nu=1$ and different average values $\langle\Gamma_{\alpha c}\rangle$. Using a Monte Carlo method, it has been shown [27] that this convolution does not have to be calculated but that instead Eq. (1), after the partial width $\Gamma_{\alpha c}$ and its average $\langle\Gamma_{\alpha c}\rangle$ are replaced by their corresponding total values $\Gamma_\alpha$ and $\langle\Gamma_\alpha\rangle$, can be used to describe the distribution of total $\alpha$ widths, albeit with an effective degrees of freedom,

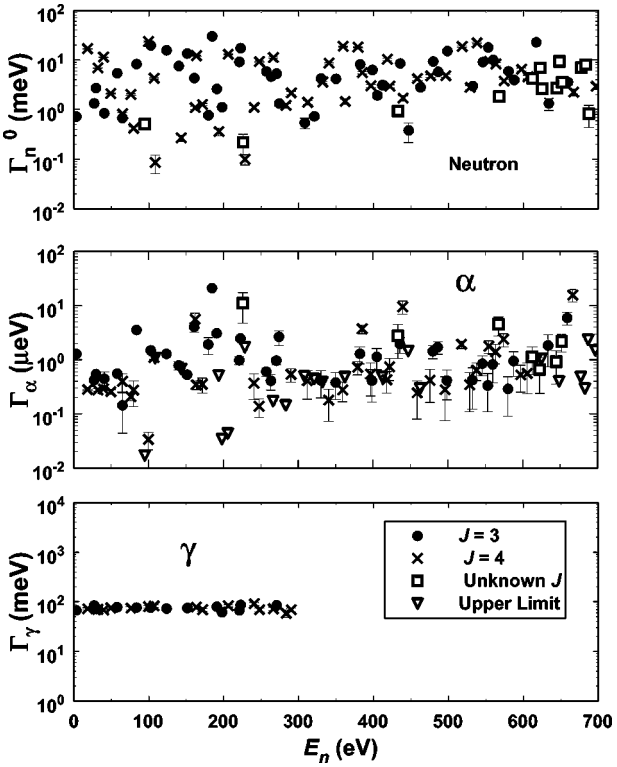


FIG. 8. Reduced neutron (top), $\alpha$ (middle), and $\gamma$ (bottom) widths for $^{147}$Sm resonances versus neutron energy. The reduced neutron and $\gamma$ widths are from previous work as compiled in Ref. [17], whereas the $\alpha$ widths are from the present work. Measured widths with $J=3$, 4, or unknown spin assignments are shown as circles, Xs, and squares, respectively. $\alpha$ widths for which only upper limits were determined are plotted as triangles.

$$\nu_{eff} = \frac{\left(\sum P_c\right)^2}{\sum P_c^2}, \qquad (2)$$

where $P_c$ is the penetrability for $\alpha$ particles in channel $c$. In the present case, the calculated [5] degrees of freedom are $\nu=1.8$ and 2.5 for $3^-$ and $4^-$ resonances, respectively. Therefore, it is expected that the fluctuations in the total $\alpha$ widths will be intermediate between that for neutrons and $\gamma$s. However, as shown in Fig. 8, although the neutron and $\gamma$ widths fluctuate as expected, the $\alpha$ widths do not appear to follow the expected behavior. For example, instead of being intermediate to the $\gamma$ and neutron distributions, the $\alpha$ widths show the largest fluctuations. Also, there appear to be regions of energy in which the $\alpha$ widths fluctuate about as expected and other regions of much larger widths and/or fluctuations. These effects are evident for both $J^\pi=3^-$ and $4^-$ resonances.

Recasting the data into plots of the cumulative widths versus resonance energy, as shown in Fig. 2 further illustrates that whereas the neutron widths behave as expected, the $\alpha$ widths show indications of nonstatistical effects. The large steps in the cumulative distributions of the $\alpha$ widths might be indications of states in $^{148}$Sm with nonstatistical properties.

Converting the data to the integral width distributions shown in Fig. 3 allows a more quantitative comparison with theory. In the case of neutrons, the widths are expected to follow Porter-Thomas distributions with average widths calculated from the measured strength functions and level spacing. As shown in the bottom part of Fig. 3, there is good agreement between the observed and expected width distributions for neutrons indicating that the neutron widths behave as expected when separated according to spin. The fit to the Porter-Thomas distribution for $J=3$ resonances can be improved by assuming additional missed resonances and hence a smaller average reduced neutron width for this spin. This indication that there may be slightly more $J=3$ resonances than the simple $2J+1$ assumption we used is in agreement with the relative sizes of the level spacings predicted in NON-SMOKER (see Sec. VI) for the two *s*-wave spin states.

Because missed resonances are expected to have random $\alpha$ widths, simple averages over the measured widths should yield good estimates of the average widths and it should be possible to compare to the expected $\chi^2$ distributions without correcting for missed resonances. These comparisons are shown in the top of Fig. 3. For the theoretical $\chi^2$ distributions, average $\alpha$ widths were calculated from simple averages of the widths determined in the resonance analysis and the degrees of freedom values were taken from Ref. [5]. In an attempt to depict the uncertainties in the $\Gamma_\alpha$ values, two histogram curves are plotted in each part of Fig. 3 corresponding to the $\alpha$ widths plus and minus their uncertainties. Resonances for which only upper limits were determined are plotted at the fitted values plus and minus their uncertainties as determined by SAMMY. For the 44 firm $3^-$ resonances $\langle\Gamma_\alpha\rangle=1.50$ $\mu$eV, whereas for the 45 firm $4^-$ resonances $\langle\Gamma_\alpha\rangle=1.24$ $\mu$eV. As shown in Fig. 3, the theoretical distributions are substantially different from the data. Furthermore, the agreement cannot be improved by, for example, decreasing the average widths and increasing the number of resonances in an attempt to correct for possible effects due to missed resonances. On the other hand, for $J^\pi=3^-$ resonances it is possible to obtain fairly good agreement between the data and the theoretical distribution if the resonance with the largest $\alpha$ width at 184.76 eV is excluded (resulting in $\langle\Gamma_\alpha\rangle=1.05$ eV and $N=43$). For $J^\pi=4^-$ resonances however, reasonably good agreement can be obtained only if 3–4 resonances with the largest $\alpha$ widths are excluded. These are the same resonances that cause the large steps in the top part of Fig. 2.

One final piece of evidence on the unusual nature of the extracted $\alpha$ widths is revealed in a comparison of the average widths for resonances for the two different spins. In the energy range of this work, emitted $\alpha$ particles from the $^{147}$Sm$(n,\alpha)$ reaction are below the Coulomb barrier, so penetrability is a steep function of energy. Therefore, the average $\alpha$ width for $3^-$ resonances is expected to be 5–10 times larger than for $4^-$ resonances because the latter are forbidden by parity conservation from decaying to the $0^+$ ground state of $^{144}$Nd (and hence on average have less energy), whereas the former are not. However, as noted above, the $\alpha$ widths averaged over all resonances with firm spin assignments are almost equal for the two spin states. Furthermore, the $\alpha$ strength functions for the two spins are expected to remain constant over the range of our resonance analysis given the smallness of our range of neutron energies compared to the energies of the emitted $\alpha$ particles ($Q_{(n,\alpha)}=10.127$ MeV). However, as can be seen in Fig. 5, our data reveal a striking disagreement with the expectations. We find that the ratio of $\alpha$ strength functions for the two spin states changes rather dramatically from $\approx 3$ to $\approx 0.5$ near $E_n=300$ eV.

## VI. COMPARISON TO THEORY

Even though the data show signs of nonstatistical effects, it is interesting to compare the measured average resonance parameters to those computed from optical potentials. Although this is independent of the Hauser-Feshbach approach, using potentials similar to those from established statistical models allows a direct test of the potentials and an examination of the various components contributing to the calculated cross section, and also should yield a better understanding of nonstatistical signatures.

### A. Definitions

The statistical model (Hauser-Feshbach approach) [28,29] assumes the compound nucleus reaction mechanism and a nuclear level density sufficiently high to be able to average across it. In this approach, the cross section between a target nucleus $i$ and projectile $j$ proceeding to exit channel $e$ (i.e., the $\alpha$ channel in our case) is given by

$$\sigma^{\mathrm{HF}} = \frac{\pi^2}{k_j^2}\frac{(1+\delta_{ij})}{(2I_i+1)(I_j+1)}\sum_{J,\pi}(2J+1) \times \frac{T_j(E,J,\pi)T_e(E,J,\pi)}{T^{\mathrm{tot}}(E,J,\pi)}W_{j,e}(E,J,\pi). \quad (3)$$

In this equation, $k_j$ is the wave number of the projectile, $I_i$ and $I_j$ are the spins of the target and projectile, respectively, and the transmission coefficients (TCs) $T(E,J,\pi)$ and width fluctuation corrections (WFC) $W_{j,e}(E,J,\pi)$ are defined by [29]

$$T(E,J,\pi) = \frac{2\pi}{D(E,J,\pi)}\langle\Gamma_{J,\pi}(E)\rangle, \quad (4)$$

and

$$W_{j,e}(E,J,\pi) = \left\langle \frac{\Gamma_{j,J,\pi}(E)\Gamma_{e,J,\pi}(E)}{\Gamma^{\mathrm{tot}}_{J,\pi}(E)} \right\rangle \frac{\langle\Gamma^{\mathrm{tot}}_{J,\pi}(E)\rangle}{\langle\Gamma_{j,J,\pi}(E)\rangle\langle\Gamma_{e,J,\pi}(E)\rangle}. \quad (5)$$

The decaying compound nucleus is characterized by the average level spacing $D(E,J,\pi)$ of states with spin $J$ and parity $\pi$ at the excitation energy $E$. Note that in the laboratory $T_j$ contains only the transition to the ground state of the target, whereas $T_e$ contains a sum over all possible transitions in the exit channel. The WFC correlate the incoming and outgoing channels and account for preequilibrium effects ($W_{j,e}\leqslant 1$) by rearranging the flux into different channels. In practice, they usually are implemented by applying corrections to the cal-

culated widths. For our case it is important to note the difference between widths obtained with or without WFC. The WFC are a model effect. Therefore, widths calculated *without* WFC should be used when comparing to directly measured widths. These are the averaged widths $\langle\Gamma\rangle$ found in the above equations. However, in the calculation of statistical model cross sections, the WFC are important and must be included. For the $(n, \alpha)$ energy range studied here, this strongly affects the neutron channel, introducing a further uncertainty in the theoretical modeling of the cross section. Nevertheless, the WFC are generally thought to be well understood.

The strength functions $S$ extracted from the experimental data are closely related to the theoretical TCs,

$$S(E, J, \pi) = \frac{T(E, J, \pi)}{2\pi}, \tag{6}$$

and generally include all energetically and spin-algebraically allowed transitions from the compound state $(E, J, \pi)$ to the final states. As seen in Fig. 6, this includes the $\alpha_0$, $\alpha_1$, $\alpha_2$, … transitions in the $\alpha$ channel for the $3^-$ compound resonances but excludes the $\alpha_0$ transition for the $4^-$ resonances. In the calculation, above the first 10 excited states in $^{144}$Nd the sum over individual states is replaced by an integration over a level density in $^{144}$Nd. However, in the present case most of the contribution to the total TC (or strength function) arises from the lowest-lying states included explicitly. Thus, any possible error in the level density in the final nucleus is strongly suppressed and does not affect the TCs.

The TC for a given transition with specified quantum numbers is computed by solving the stationary Schrödinger equation with a given optical potential. Thus, the TCs are sensitive only to the optical potential.

It becomes evident from the considerations above that, when possible, it is preferable to compare calculated TCs to strength functions extracted from experimental data. The TCs are primary quantities depending only on the optical potential; thus, this approach makes it possible to disentangle the various contributions to the theoretical uncertainty. Converting strength functions to theoretical widths adds the uncertainty in the compound level density $\rho(E, J, \pi) = 1/D(E, J, \pi)$. Comparing cross sections includes all possible errors in the widths of the different channels (optical potentials), the level density, and the WFC.

### B. Comparison of strength functions

Strength functions calculated employing the same methods used in the statistical model code NON-SMOKER [30–32] are compared to the data in Figs. 4 and 5 and Table II. These calculations were made to illuminate the various confounding effects that enter into calculations of cross sections and reaction rates as well as to ascertain whether it is possible to reproduce the data using optical model strength functions, especially given the indications of nonstatistical effects noted above.

Several differently parametrized potentials are available in literature, but for simplicity we limit our investigation to one basic shape (Woods-Saxon) and two basic parameter sets; the one of Ref. [33] (potential $P1$, standard NON-SMOKER settings) and the other from Refs. [34–36] (potential $P2$). Cross sections for the $^{147}$Sm$(n, \alpha)^{144}$Nd reaction calculated using potential $P1$ are a factor of 3.3 larger than the data [3], whereas calculations made using potential $P2$ are in significantly better agreement (a factor of 1.4 higher than the data) with these data as well as data from a number of other reactions.

TABLE III. Parameter of the basic Woods-Saxon potentials.

| Potential | $V$ MeV | $r_r$ fm | $a_r$ fm | $W$ MeV | $r_i$ fm | $a_i$ fm |
|---|---|---|---|---|---|---|
| $P1$ [33] | 185.0 | 1.40 | 0.52 | 25.0 | 1.4 | 0.52 |
| $P2$ [34–36] | 162.3 | 1.27 | 0.48 | 25.0 | 1.4 | 0.52 |

Both potentials use standard Woods-Saxon shapes in the real and imaginary parts of the radial potential $U$,

$$U(r) = -\frac{V}{1+\exp\left(\frac{r - r_r A^{1/3}}{a_r}\right)} - i\frac{W}{1+\exp\left(\frac{r - r_i A^{1/3}}{a_i}\right)}. \tag{7}$$

The parameters are given in Table III. It is interesting to note that the imaginary parts of the two potentials are the same. Nevertheless, $P2$ yields a value closer to the measured cross section. At first glance, this seems counterintuitive as it is commonly stated that the imaginary part of the optical potential determines the TC. However, it is more correct to state that the TC is given by the imaginary part of the wave function which in turn depends on the relative strengths of the real and the imaginary parts of the potential.

As can be seen, the calculated strength functions in the neutron channel are about a factor of 2 larger than experiment for both $3^-$ and $4^-$ resonances. It is interesting to note that the standard NON-SMOKER [31] level spacings ($D_0 = 7.4$ and 6.5 eV for $J = 3$ and 4 resonances, respectively) are about a factor of 2 smaller than the measured ones; hence, the calculated average neutron widths are in fairly good agreement with the measured values. This illustrates the importance of making the comparison between theory and experiment as strength functions, for if instead average widths were compared, the confounding influence of the level spacing might lead one to conclude that there was better agreement between theory and experiment than there actually is.

For potential $P1$, in the $E_n = 0-300$ eV range, the calculated $4^-$ $\alpha$ strength function is about a factor of 2 larger than measured, but the calculated $\alpha$ strength function for $J^\pi = 3^-$ is in more serious disagreement (a factor of about 6 larger) with experiment. In the $E_n = 300-600$ eV range, the $4^-$ $\alpha$ strength function calculated with potential $P1$ is in good agreement with the data, but for $3^-$ resonances the $\alpha$ strength function is in even more serious disagreement (about a factor of 17) than it was in the lower-energy region. Potential $P2$ is clearly better than $P1$ in predicting the $\alpha$ strength function for $3^-$ resonances and for $4^-$ resonances in the $E_n = 0-300$ eV re-

gion. However, as shown in Fig. 5, both potentials strongly overpredict the $3^- - 4^-$ $\alpha$ strength function ratio, potential $P2$ yielding a ratio only slightly smaller than that calculated with potential $P1$.

These comparisons as strength functions indicate that the optical $\alpha + {}^{144}$Nd potential requires more adjustment than would be surmised from comparisons as cross sections. However, it should be noted that the cross-section comparisons were made at higher energies ($E_n \approx 10-500$ keV) where contributions from $p$-wave resonances are expected to become more important. Furthermore, the disagreement between calculated and actual strength functions might become smaller at higher energies as has been found in other reactions. Nevertheless, it is informative that both the calculated neutron and $\alpha$ strength functions are too large—a fact that could not be surmised from comparisons as ${}^{147}\mathrm{Sm}(n, \alpha){}^{144}\mathrm{Nd}$ cross sections.

As shown in Fig. 5, the ratio of the calculated $\alpha$ strength functions for the two $s$-wave spin states is constant over the energy range of resonance analysis. This is in stark contrast to the measurements which show a steep decrease in this ratio above $E_n = 300$ eV. Regardless of the potential used, it will never be possible to achieve such an abrupt change in the ratio within an optical model of strength functions. However, it is possible that the abrupt change in the $3^- - 4^-$ $\alpha$ strength function ratio is due to incorrect spin assignments above $E_n = 300$ eV. Therefore, it is interesting to study if calculations can reproduce the measured ratio below $E_n = 300$ eV where the data should be very reliable. Two conclusions can be drawn from a more systematic variation of the parameters of a Woods-Saxon $\alpha$ potential which we attempted. First, the absolute values of the strength functions are far more sensitive to the potential than is the $3^- - 4^-$ $\alpha$ strength function ratio. Trying to reduce to calculated ratio by only the smaller amount needed to reproduce the measured ratio in the region below $E_n = 300$ eV quickly leads to strength functions which are orders of magnitude larger than the observed ones (and hence also to an inferior description of the cross section). Second, it is impossible to obtain a $3^- - 4^-$ $\alpha$ strength function ratio smaller than unity with any Woods-Saxon potential. In consequence, it is impossible to reproduce the small ratio observed above $E_n = 300$ eV with any such calculation. Thus, from this analysis it appears that a $3^- - 4^-$ $\alpha$ strength function ratio smaller than unity may be an additional indication of a nonstatistical effect in the data.

Finally, the NON-SMOKER calculation predicts that 78% of the ${}^{147}\mathrm{Sm}(n, \alpha){}^{144}\mathrm{Nd}$ cross section is given by transitions from $3^-$ states, 12% from $4^-$ states, and 10% from other states (higher partial waves). Of the $3^-$ transitions, 67% directly populate the ground state of ${}^{144}$Nd, which cannot be reached from $4^-$ resonances. New measurements in which the various $\alpha$ groups are resolved would be very useful for testing these predictions. The relative contributions of the various transitions also shows why it is more important for cross section predictions to reproduce the $3^-$ TCs than the $3^- - 4^-$ ratio. Therefore, potential $P2$, which has essentially the same $3^- - 4^-$ ratio as potential $P1$ but comes much closer to reproducing the $3^-$ TCs, yields a cross section in better agreement with the measurements.

## VII. CONCLUSION

Comparing theory to experiment as $\alpha$ strength functions rather than as ${}^{147}\mathrm{Sm}(n, \alpha)$ cross sections avoids confounding effects due to the neutron and $\gamma$ channels, level densities, and width fluctuation corrections and therefore can reveal more useful information about possible improvements to theoretical models by isolating effects due to the $\alpha$+nucleus potential. Furthermore, separating the data into the two possible $s$-wave spin states may yield even more information about the $\alpha$+nucleus potential, because $\alpha$ particles from $3^-$ resonances have (on average) larger energies than those from $4^-$ resonances and hence they sample a different region of the $\alpha$+nucleus potential. Therefore, differences between the measured and calculated $\alpha$ strength functions for the two different $s$-wave spin states should be useful for future improvements in the $\alpha$+nucleus potential. An improved $\alpha$ +nucleus potential would be very useful for astrophysical applications.

Interestingly, it is clear from the data presented in Fig. 8 that the extracted $\alpha$ widths exhibit fluctuations different from the expected behavior and hint at possible nonstatistical effects. One striking feature is that the $\alpha$ widths exhibit peaks and/or regions of large fluctuations as a function of neutron energy instead of the expected random fluctuations intermediate to that for neutron and $\gamma$ widths. Perhaps these peaks are a manifestation of a nuclear structure effect in the ${}^{148}$Sm compound nucleus that is not observable in decay channels other than the $\alpha$ channel. One important difference between the decay of the ${}^{148}$Sm compound nucleus into the $\alpha$ channel compared to decay into the neutron or $\gamma$ channels is the large Coulomb barrier that the $\alpha$ particles must overcome. Hence, it is possible that the Coulomb barrier for $\alpha$ decay could act as a lever arm enhancing the signature of nuclear structure effects that are too subtle to be observed in other channels. For example, $\alpha$ decay could be enhanced for compound states with significant deformation and for $J^\pi = 4^-$ states of significant collectivity (because they decay mainly to the $I^\pi = 2^+$ first excited state of ${}^{144}$Nd).

Further evidence for possible nonstatistical behavior of the $\alpha$ widths is revealed when the resonances are separated according to spin as shown in Figs. 2–5. The striking disagreement with theoretical expectations shown in these figures depends on reliable spin assignments for the resonances. The spin assignments used in these figures rely on the results of Ref. [18], the good match between the energy scale for this reference and our work, and the crude pulse-height information from our experiment for resonances having large $\alpha$ widths. Below $\approx$300 eV, the spin assignments used herein should be very reliable. Therefore, it is very interesting that our exploratory calculations show that, even in this energy range, it is not possible to reproduce the observed $\alpha$ strength functions as well as the $3^- - 4^-$ $\alpha$ strength ratio at the same time using a Woods-Saxon potential.

The $\alpha$-width distributions shown in Figs. 2 and 3, as well as the striking change in the $3^- - 4^-$ $\alpha$ strength ratio near 300 eV shown in Fig. 5 depend on reliable spin assignments above 300 eV. For a number of reasons, the spin assignments in this region may not be as reliable, so it would be very useful to make new ${}^{147}\mathrm{Sm}(n, \alpha)$ measurements with

thinner samples to check spin assignments, especially for those resonances having the largest $\alpha$ widths. In such measurements, resonances having visible $\alpha_0$ groups to the ground state of $^{144}$Nd unambiguously could be assigned as $J=3$. The $\alpha$-particle spectra for the few resonances below $E_n=185$ eV that have been reported [4] are in agreement with the accepted [17] spin assignments, except possibly the 58.130-eV resonance (57.9 eV in Ref. [4]), which is assigned $J^\pi=3^-$ but has an almost invisible $\alpha_0$ group. New neutron capture and total cross-section measurements on $^{147}$Sm also could be useful. New measurements with higher resolution and sensitivity could reduce uncertainties in the $\alpha$ widths by identifying some of the missing resonances in the relevant energy range and by providing more $\gamma$ widths as well as more precise neutron widths. Finally, $(n, \alpha)$, $(n, \gamma)$, and neutron total cross sections on other nuclides in this mass region should be very useful in shining more light on this interesting problem.

## ACKNOWLEDGMENTS

We would like to thank J. A. Harvey, J. E. Lynn, Yu. P. Popov, S. Raman, and F.-K. Thielemann for fruitful discussions. This work was supported in part by the U.S. Department of Energy under Contract No. DE-AC05-00OR22725 with UT-Battelle, LLC, and by the Swiss NSF (Grant No. 2000-061031.02). T.R. acknowledges support from the Swiss NSF (Grant No. 2024-067428.01).

[1] R. D. Hoffman, S. E. Woosley, T. A. Weaver, T. Rauscher, and F.-K. Thielemann, Astrophys. J. **521**, 735 (1999).
[2] T. Rauscher, A. Heger, R. D. Hoffman, and S. E. Woosley, Astrophys. J. **576**, 323 (2002).
[3] Y. M. Gledenov, P. E. Koehler, J. Andrzejewski, K. H. Guber, and T. Rauscher, Phys. Rev. C **62**, 042801(R) (2000).
[4] Y. P. Popov, M. Przytula, R. F. Rumi, M. Stempinski, and M. Frontasyeva, Nucl. Phys. **A188**, 212 (1972).
[5] N. P. Balabanov, Y. M. Gledenov, P. H. Chol, Y. P. Popov, and V. G. Semenov, Nucl. Phys. **A261**, 35 (1976).
[6] Y. Andzheevski, V. K. Tkhan', V. A. Vtyurin, A. Koreivo, Y. P. Popov, and M. Stempin'ski, Yad. Fiz. **32**, 1496 (1980).
[7] A. Antonov, Y. M. Gledenov, S. Marinova, Y. P. Popov, and H. Rigol, Yad. Fiz. **39**, 794 (1984).
[8] J. Kvitek and Y. P. Popov, Nucl. Phys. **A154**, 177 (1970).
[9] W. Rapp, P. E. Koehler, F. Käppeler, and S. Raman, Phys. Rev. C **68**, 015802 (2003).
[10] R. W. Peelle, J. A. Harvey, F. C. Maienschein, L. W. Weston, D. K. Olsen, D. C. Larson, and R. L. Macklin, Oak Ridge National Laboratory Technical Report ORNL/TM-8225, 1982.
[11] K. Bockhoff, A. D. Carlson, O. A. Wasson, J. A. Harvey, and D. C. Larson, Nucl. Sci. Eng. **106**, 192 (1990).
[12] K. H. Guber, D. C. Larson, P. E. Koehler, R. R. Spencer, S. Raman, J. A. Harvey, N. W. Hill, T. A. Lewis, and R. R. Winters, in *International Conference on Nuclear Data for Science and Technology*, edited by G. Reffo, A. Ventura, and C. Grandi (Societa Italiana di Fisica, Bologna, 1997), p. 559.
[13] P. E. Koehler, J. A. Harvey, and N. W. Hill, Nucl. Instrum. Methods Phys. Res. A **361**, 270 (1995).
[14] A. D. Carlson, W. P. Poenitz, G. M. Hale, R. W. Peele, D. C. Dodder, C. Y. Fu, and W. Mannhart, National Institute of Standards and Technology Technical Report NISTIR-5177, 1993.
[15] J. F. Ziegler and J. P. Biersack, computer code SRIM 2000 (1999).
[16] N. M. Larson, Oak Ridge National Laboratory Technical Report ORNL/TM-2000/252, 2000.
[17] S. I. Sukhoruchkin, Z. N. Soroko, and V. V. Deriglazov, *Low Energy Neutron Physics* (Springer-Verlag, Berlin, 1998).
[18] G. Georgiev, Y. S. Zamyatnin, L. B. Pikelner, G. V. Muradian, Y. V. Grigoriev, T. Madjarski, and N. Janeva, Nucl. Phys. **A565**, 643 (1993).
[19] J. J. W. Codding, R. L. Tromp, and F. B. Simpson, Nucl. Sci. Eng. **43**, 58 (1971).
[20] H. M. Eiland, S. Weinstein, and K. W. Seeman, Nucl. Sci. Eng. **54**, 286 (1974).
[21] M. Mizumoto, Nucl. Phys. **A357**, 90 (1981).
[22] S. F. Mughabghab, *Neutron Cross Sections* (Academic, New York, 1984).
[23] S. F. Mughabghab, M. Divadeenam, and N. E. Holden, *Neutron Cross Sections* (Academic, New York, 1981), Vol. 1.
[24] C. E. Porter and R. G. Thomas, Phys. Rev. **104**, 483 (1956).
[25] Y. M. Gledenov, P. E. Koehler, J. Andrzejewski, Y. P. Popov, and R. Y. Gledenov, Nucl. Sci. Technol. **1**, Suppl. 2, 358 (2002).
[26] P. E. Koehler, Y. M. Gledenov, J. Andrzejewski, K. H. Guber, S. Raman, and T. Rauscher, Nucl. Phys. **A688**, 86c (2001).
[27] Y. P. Popov, M. Prztula, R. F. Rumi, M. Stempinski, M. Florek, and V. I. Furman, *Nuclear Data for Reactors* (International Atomic Energy Agency, Vienna, 1970), p. 669.
[28] W. Hauser and H. Feshbach, Phys. Rev. **87**, 366 (1952).
[29] E. Gadioli and P. E. Hodgson, *Pre-Equilibrium Nuclear Reactions* (Clarendon, Oxford, 1992).
[30] T. Rauscher and F.-K. Thielemann, in *Stellar Evolution, Stellar Explosions, and Galactic Chemical Evolution*, edited by A. Mezzacappa (IOP, Bristol, 1998), p. 519.
[31] T. Rauscher and F.-K. Thielemann, At. Data Nucl. Data Tables **75**, 1 (2000).
[32] T. Rauscher and F.-K. Thielemann, At. Data Nucl. Data Tables **79**, 47 (2001).
[33] L. McFadden and G. R. Satchler, Nucl. Phys. **84**, 177 (1966).
[34] C. Fröhlich, diploma thesis University of Basel, Switzerland.
[35] T. Rauscher, C. Fröhlich, K. H. Guber, in *Capture Gamma-Ray Spectroscopy and Related Topics*, edited by J. Kvasil, P. Cejnar, and M. Krticka (World Scientific, Singapore, 2003), p. 781; nucl-th/0302046.
[36] T. Rauscher, Nucl. Phys. **A719**, 73c (2003); **A725**, 295(E) (2003).